



Operando Temperature Dynamic Investigation of Electric Double-Layer Capacitors Containing Organic Electrolytes

Fabian Alexander Kreth^{+[a]}, Lukas Köps^{+[a]}, Scott W. Donne,^[b] and Andrea Balducci*^[a]

Variations in temperature play a substantial role in influencing the electrochemical performance of electric double-layer capacitors (EDLCs). Lower temperatures limit the charge carriers' transport properties, diminishing overall cell performance, while higher temperatures enhance transport properties and performance at the expense of material decomposition. Thus, investigating the temperature-dependent behavior of supercapacitors requires numerous time-consuming experiments while maintaining specific and consistent testing conditions. Therefore, we present a fast screening technique, named operando temperature dynamic measurements, to investigate EDLC performance under varying temperatures and voltages. The

swift nature of this technique minimizes cell aging, allowing the evaluation even at harsh conditions. Utilizing temperature dynamic measurements, EDLCs containing six different organic electrolytes have been compared. Incrementally increasing temperature and cell voltage while performing electrochemical impedance spectroscopy or galvanostatic charge-discharge measurements, metrics such as capacitance, energy, power, entropy, and enthalpy were determined. Interestingly, different performance evolutions over the temperature range are observed, allowing the identification of optimal operational conditions for each device.

1. Introduction

As society continues to shift towards renewable energy, the role of electrochemical energy storage devices that can rapidly uptake and deliver energy has become increasingly important. Supercapacitors, especially electric double-layer capacitors (EDLCs), have gained attention due to their high power density, long cycle life, and low internal resistance. These properties make them the optimal choice for a large number of applications in electric vehicles, renewable energy systems, and consumer electronics in which low amount of energy, but high power and high reliability are needed.^[1]

It is important to remark that in many of these applications a significant amount of heat under high loads can be generated, which can limit the performance and lifetime of EDLCs.^[2] Commercial EDLCs contain electrolytes based on organic solvents (typically acetonitrile, ACN), which exhibit low boiling point and high volatility. At elevated temperatures, the electrolyte solvent undergoes evaporation and degradation,

leading to several adverse effects. Firstly, it diminishes cell performance due to a reduction in the number of liquid solvent molecules and the blockage of pores caused by the adsorption of gaseous solvent molecules. Moreover, solvent evaporation poses safety concerns by increasing internal pressure, which can lead to venting or even cell explosion. Furthermore, higher temperatures accelerate unwanted side reactions by providing the necessary activation energy for specific decomposition reactions. This also facilitates quicker movement of reactants towards the electrode surface and the removal of products from the electrode surface. Hence, it is crucial to consider the electrochemical and chemical stability of novel electrolytes for EDLCs, particularly when exposed to elevated temperatures.^[3]

As mentioned above, commercial EDLCs typically contain ACN as solvent. Some devices have been also realized utilizing propylene carbonate (PC). Independently on the used solvent, tetraethylammonium tetrafluoroborate (TEABF₄) is usually used as the electrolyte salt.^[4] Utilizing these solvent-salt combination it is possible to realize EDLCs with operating voltages in the range of 2.7–3.0 V. In recent years, several alternative solvents have been proposed for the application in EDLCs, such as adiponitrile (ADN), propionitrile (PN), butylenecarbonate (BC), and γ -valerolactone (GVL). In combination with those solvents, a variety of quaternary ammonium or pyrrolidinium-based salts (R_4N^+ or Pyr_{RR'}⁺), mostly paired with tetrafluoroborate (BF₄⁻) or bis(trifluoromethanesulfonyl)imide (TFSI⁻), have been proposed as potential alternatives.^[1C,5] Especially noteworthy is the application of 1,1-dimethylpyrrolidinium tetrafluoroborate (Pyr₁₁BF₄) as conducting salt, which enables an increase in operating voltage of ACN-based system from 3.0 V up to 3.4 V.^[3]

Although the performance of EDLCs containing these alternative solvents and salts has been studied quite extensively, a systematic investigation of the impact of temperature on their electrochemical behavior currently appears to be of

[a] F. A. Kreth,^{+[a]} L. Köps,^{+[a]} A. Balducci

Friedrich-Schiller-University Jena, Institute for Technical Chemistry and Environmental Chemistry (ITUC) and Center for Energy and Environmental Chemistry Jena (CEEC Jena), Philosophenweg 7a, 07743 Jena, Germany
E-mail: andrea.balducci@uni-jena.de

[b] S. W. Donne

Discipline of Chemistry, University of Newcastle, Callaghan NSW 2308, Australia

[+] These authors contributed equally.

Supporting information for this article is available on the WWW under <https://doi.org/10.1002/batt.202300581>

© 2024 The Authors. *Batteries & Supercaps* published by Wiley-VCH GmbH. This is an open access article under the terms of the Creative Commons Attribution Non-Commercial License, which permits use, distribution and reproduction in any medium, provided the original work is properly cited and is not used for commercial purposes.

great importance. In particular, the interrelation between operating temperature and applied cell voltage appears to be one of the most important aspects to understand, as it affects the development and design of EDLCs.

Intending to address this important point, in this work we report a systematic electrochemical investigation, carried out using operando temperature dynamic measurement, highlighting how the operating temperature influences the performance of electric double-layer capacitors (EDLCs) using various electrolytes.

2. Results and Discussion

An ideal electrolyte for EDLC should exhibit high thermal stability and ionic conductivity, as well as low viscosity. It is well known that it is very difficult to obtain all these properties simply by mixing a salt with a solvent, and that neither commercial nor alternative electrolytes proposed so far exhibit all these characteristics. Figure 1 compares the ionic conductivity (σ), viscosity (η) and the thermal behavior (in terms of relative mass m) of the six different electrolytes considered in this study, which consists of a 1 M solution of $\text{Pyr}_{11}\text{BF}_4$ dissolved in ACN, PN, ADN, PC, BC and GVL (see Scheme 1 of the Experimental Section). By comparison of the transport properties, it is evident that for all electrolytes the ionic conductivity increases while the viscosity decreases at higher temperatures. Although this indicates a better ion mobility with increasing temperature, their thermal stability needs to be considered. As shown in Figure 1c, all electrolytes show a steep decrease in relative mass before reaching a plateau. This is caused by the loss of the respective organic solvent. The lower the volatility of a solvent the later its evaporation occurs. After this initial mass loss a plateau associated to the thermal stability of the salt $\text{Pyr}_{11}\text{BF}_4$ is visible. The respective heights of the plateaus correlate well with the density of the respective solvents. At a temperature of 500°C, all components of the investigated electrolytes are thermally decomposed. By comparison of transport properties and the thermal behavior of the electrolytes, it is evident that electrolytes that show high ionic conductivity and a low viscosity display an unfavorable low thermal stability. At the same time, electrolytes which show a high thermal stability show a high viscosity and low ionic conductivity. Whereas conductivity increases in the following order: ADN < BC < GVL < PC < PN < ACN, viscosity and thermal stability decrease in the opposite order: ACN < PN < GVL < PC < BC < ADN. Thus, it is evident, that when designing electrolytes, a good compromise between good transport properties and high stability has to be achieved.

In the past, these electrolytes have been extensively tested for potential application in EDLCs. The results, specifically focusing on long-term stability under varying voltages and temperatures, are summarized in Table S1 and comment 1 of the Supporting Information (SI).^[5B,6] It is evident that examining the performance and stability of EDLCs requires specific and consistent testing conditions throughout the entire experiment. Thus, to investigate the impact of temperature and voltage,

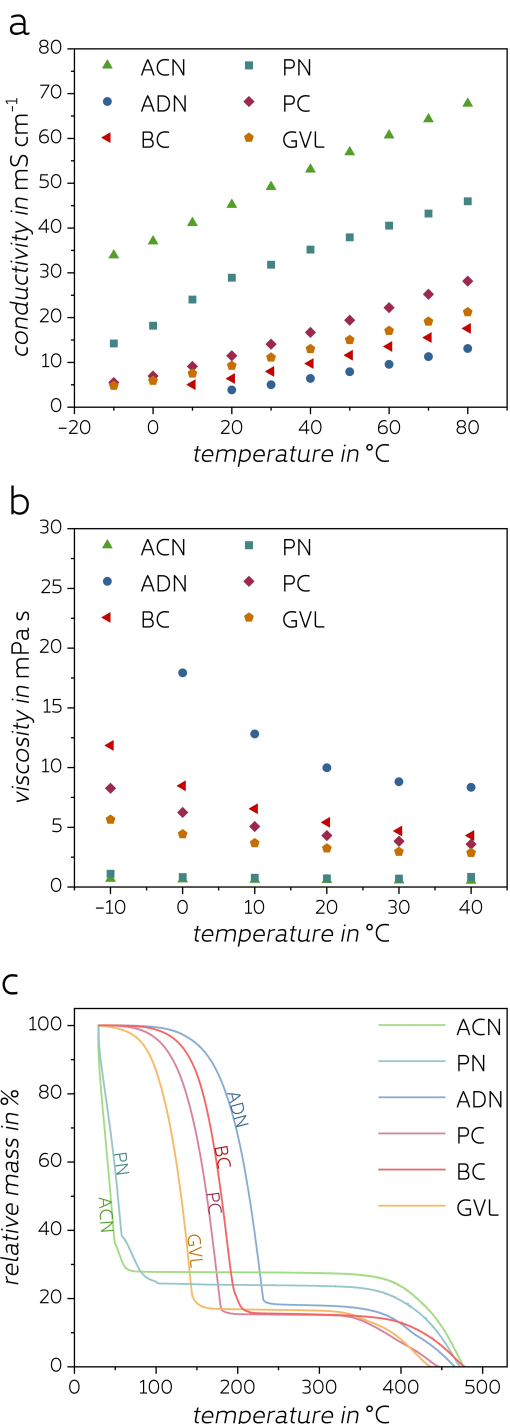
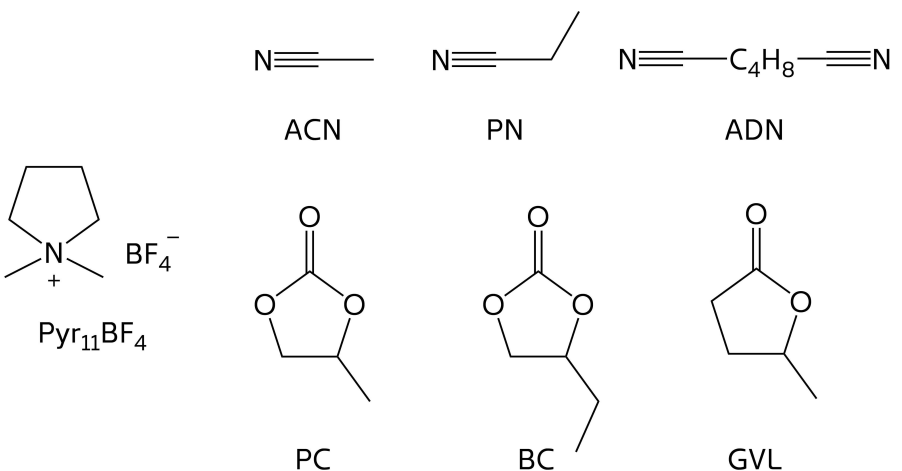


Figure 1. Physicochemical properties of the investigated electrolytes consisting of a 1 M solution of $\text{Pyr}_{11}\text{BF}_4$ in ACN (green), PN (turquoise), ADN (blue), PC (violet), BC (red), and GVL (orange). **a**) shows the ionic conductivity as a function of the temperature within a temperature range of -10°C to 80°C , **b**) shows the viscosity within a temperature range of -10°C to 50°C , and **c**) shows the thermal stability during the application of a temperature ramp from 30°C to 500°C .

numerous time-consuming measurements would be necessary. Unfortunately, there is a scarcity of data on these conditions. Therefore, we developed new and fast testing protocols, which we refer to as operando temperature dynamic measurements



Scheme 1. Chemical structures of the salts dimethylpyrrolidinium tetrafluoroborate ($\text{Pyr}_{11}\text{BF}_4$) and of the six solvents: acetonitrile (ACN), propionitrile (PN), adiponitrile (ADN), propylenecarbonate (PC), butylenecarbonate (BD), and γ -valerolactone (GVL) utilized in this study.

(T-dyn). Those enable the investigation of EDLC performance under varying temperatures and voltages, offering a swift screening process that minimizes cell aging even at harsh conditions. It is important to note that the following performance values represent a snapshot of the cell under various

conditions and do not provide insights into the respective long-term stability.

Figure 2 shows Nyquist diagrams of the performed T-dyn electrochemical impedance spectroscopy measurements (T-dyn EIS). This technique allowed us to repeatedly perform impe-

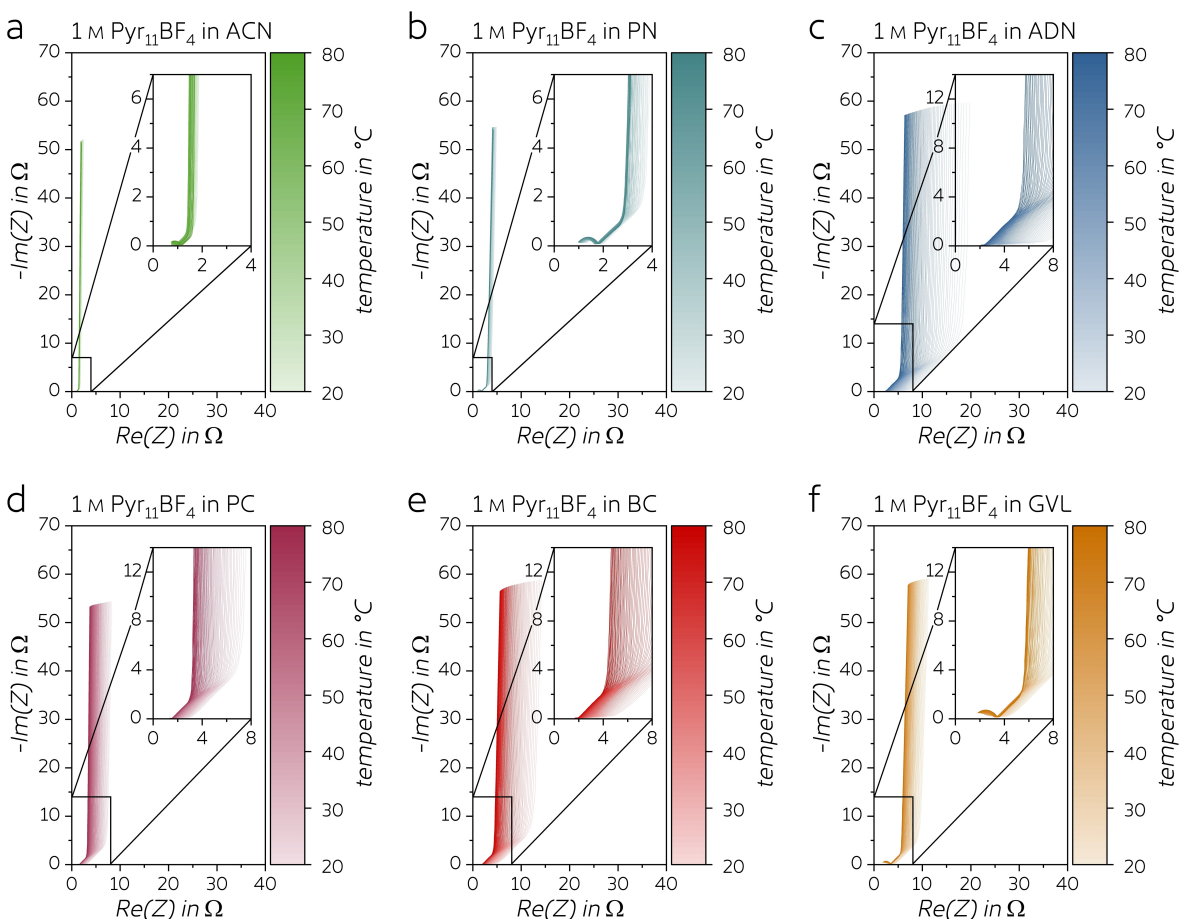


Figure 2. Influence of the temperature on the impedance of symmetric EDLCs based on a 1 M solution of $\text{Pyr}_{11}\text{BF}_4$ in a) ACN, b) PN, c) ADN, d) PC, e) BC, and f) GVL. EIS measurements are performed at open circuit voltage in a frequency range from 100 kHz – 10 mHz and a temperature range from 20–80 $^{\circ}\text{C}$.

dance measurements while increasing the temperature incrementally from 20 °C to 80 °C (in steps of 1 °C). From the figure, it is evident that the resistance values of the devices increase in the following order: ACN < PN < PC < GVL < BC < ADN. Since the differences in resistivity are primarily caused by the varying transport properties of the electrolytes, it is not surprising that this increase follows the same order as the decrease in ionic conductivity. While most of the investigated electrolytes show a decrease of the overall resistance with increasing temperature, which is indicated by the shift to lower values of the real part of the impedance, the ACN-based electrolyte shows an increase of resistance at temperatures higher than 50–60 °C. Further, an increase of temperature leads to a reduced Warburg impedance, indicating better transport properties at high temperatures. Even though the ACN-based electrolyte shows the lowest resistance and least dominant Warburg impedance, an increase of resistance at high temperatures indicates the decomposition of the respective electrode-electrolyte interphase.^[7] Leading to pore-blocking and electrolyte-depleting side reactions, ACN-based EDLCs can not be recommended for high-temperature applications. Following the part correlated to the Warburg impedance, a steep increase of the imaginary part of the impedance is observed for all electrolytes indicating capacitive behavior.

It is important to note that, while increasing the temperature, the respective resistance $Re(Z)$ shifts towards lower values, and the respective height of the capacitive tail decreases. The latter is important since a decrease of the reactance $Im(Z)$ directly correlates to a higher capacitance, energy, and power. Furthermore, electrochemical impedance spectroscopy offers a means to gain insights into the kinetics of the energy storage mechanism of an EDLC. Here, the sinusoidal signal of the current and the voltage can be considered as a recurring charge-discharge process. Thus, the reciprocal value of the applied frequency, effectively a measure of time, can be regarded as the charge-discharge time. Despite the fast nature of the formation and disintegration of electric double-layers relative to other energy storage methods, it is imperative to note that this process is not instantaneous; rather, it demands a specific duration that depends on material attributes like pore and ion dimensions, transport characteristics, and degree of solvation. Consequently, exploring the limitations of a given system holds significant importance. The specific capacitance (as defined in equation 1) can be correlated with time or frequency to quantify the extent of the respective temporal limitations. Even though it has to be acknowledged that capacitance values derived from EIS are known to yield systematically lower values compared to those measured by GCD or by cyclic voltammetry, the inherent consistency within each measurement method still permits a reliable comparative analysis (see references^[8]). Considering the electrolyte as the sole differing component, this correlation offers detailed insights into how the performance of the investigated EDLCs is influenced by the choice of solvent and the ambient temperature. Furthermore, it is important to highlight that in this work, the capacitance computation has been conducted by using the modulus function of the total impedance $|Z|$, in contrast to

solely relying on the imaginary component $Im(Z)$ (see SI, Figure S1). While in the scenario of an ideal capacitor, the real part of the impedance is insignificantly small and thus disregarded, the situation changes when comparing electrolytes that primarily vary in their transport characteristics. Here, strong variations in their real parts are observed and thus significantly impact the performance of EDLCs. As shown in Figure 3, an increase of temperature leads to an acceleration of the charge-discharge process, independently of the used electrolyte. This results in the realization of increased capacitance values within identical charge-discharge timeframes. The continuation of the trend observed at the transport properties is also evident in this context. In this regard, it is important to note that the superior performance of the ACN- and PN-based electrolytes necessitates different timeframes compared to the other electrolytes. Whereas the ACN- and PN-based electrolytes require discharge times of less than 5 s, the other electrolytes necessitate up to 20 s in order to achieve relevant capacitance values. In the case of ACN (Figure 3a), 15 F g⁻¹ can already be achieved at 20 °C within a charge storage timeframe of less than 5 s. Increasing the temperature improves transport properties, and the same value of specific capacitance can be achieved in less time (< 4 s at 50 °C). However, when exceeding 60 °C, a steep decrease in cell performance can be observed, resulting in a detrimental increase in the necessary timeframe. Compared with PN (Figure 3b), overall, less capacitance is achieved. At 20 °C, a maximum value of 10 F g⁻¹ is reached within a charge storage timeframe of approximately 5 s. Similar to ACN, a first increase of specific capacitance followed by a decrease after 60 °C is observed. Nevertheless, it is notable that PN exhibits fewer temperature dependency compared to ACN. While also belonging to the group of nitriles, ADN is much more viscous and less ionic conductive than the ones reported before (see Figure 1). This results in significantly poorer performance properties: At a temperature of 20 °C, an EDLC containing an electrolyte consisting of 1 M Pyr₁₁BF₄ in ADN barely achieves 5 F g⁻¹ within a timeframe of 10 s and not even 10 F g⁻¹ within 20 s. Remarkably, compared to ACN and PN, the cell performance continues to increase when exceeding 60 °C. In the case of the devices based on PC, BC, and GVL (Figure 3d, 3e, and 3f, respectively), the same behavior is observed, which can be attributed to the superior thermal stability of those solvents. Since the electrolyte evaporation of ACN and PN occurs around 60 °C, the remaining electrolytes show thermal stability up to more than 100 °C. In the case of the PC-based device, 10 F g⁻¹ can already be achieved at 20 °C within a charge storage timeframe of less than 10 s. Making possible the realization of EDLCs providing 15 F g⁻¹ within 20 s at 30 °C and within 10 s at 80 °C, this electrolyte shows excellent performance at high temperatures. In comparison, BC barely achieves 15 F g⁻¹ within 20 s at temperatures higher than 70 °C (Figure 3e), and GVL does not reach it at all (Figure 3f). Nonetheless, as the only representative for a sustainable solvent, GVL shows an overall good electrochemical performance while showing only a modest degree of temperature dependency.

While this technique is fast and provides a very detailed overview of the amount of charge that can be stored at a given

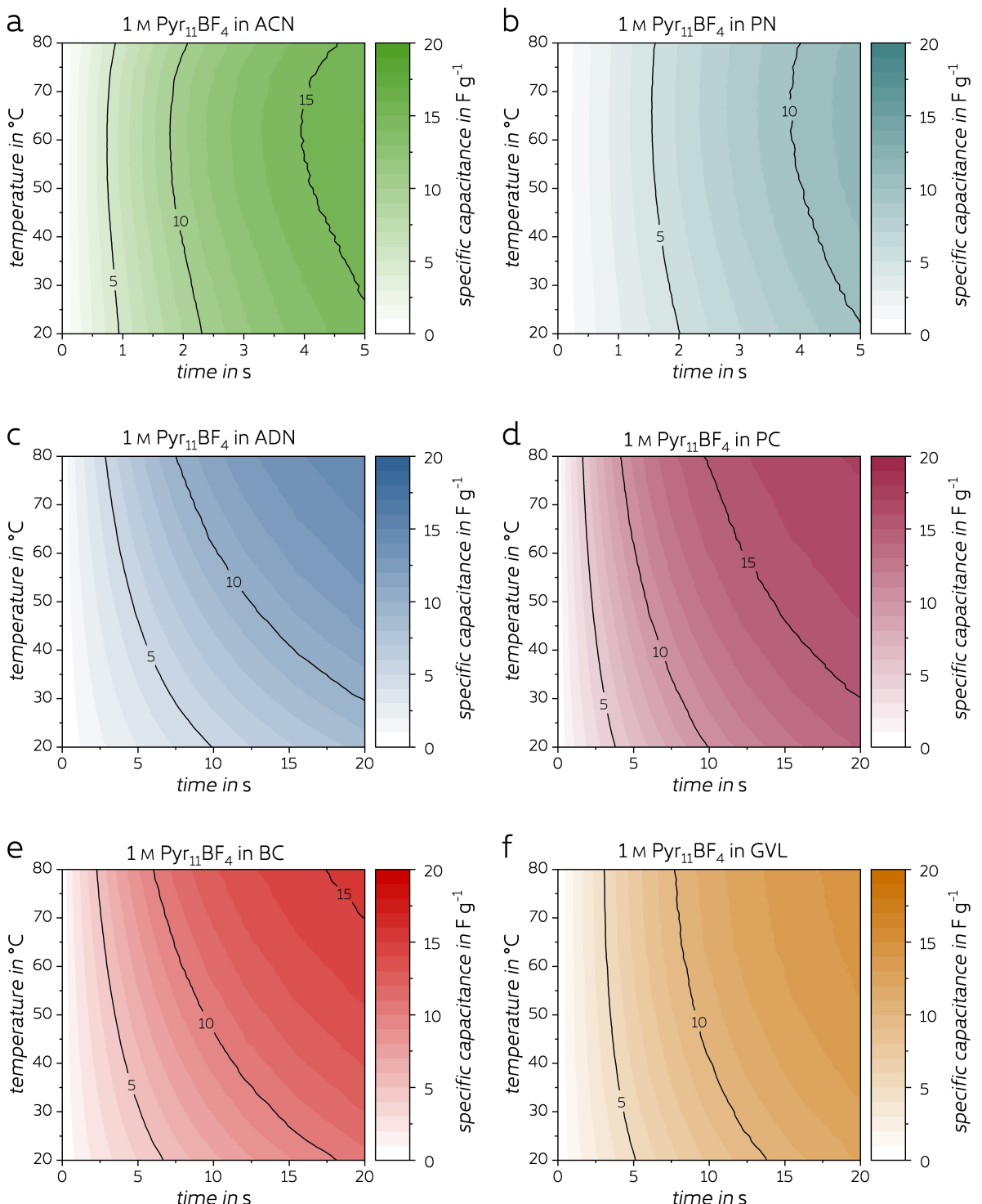


Figure 3. Evolution of the specific capacitance of a symmetrical EDLC based on 1 M solution of $\text{Pyr}_{11}\text{BF}_4$ in a) ACN, b) PN, c) ADN, d) PC, e) BC, and f) GVL. Calculated from EIS measurements in a frequency range from 100 kHz – 10 mHz and a temperature range from 20–80 °C. The shown time is derived from the reciprocal value of the frequency and therefore indicates the needed charge-discharge time. The development of the specific capacitance depending on voltage and temperature is highlighted by the black contour lines.

temperature and how fast that charge-discharge process can be conducted, it only provides limited information regarding the devices' electrochemical stability. To comprehensively address this concern, T-dyn galvanostatic charge-discharge measurements (T-dyn GCD) were performed (corresponding voltage

profiles are shown in Figure S2 of the SI). Given that the stability of an EDLC is intricately linked with the applied voltage, it becomes imperative to ascertain how voltage variations within a given temperature range impact the defining parameters of the cell. Even though the capacitance proves valuable informa-

tion for monitoring the interaction between capacitive electrode materials and electrolytes, it does not consider factors such as internal resistance and a possible non-linear dependency between the cell voltage and current (as it is the case for electron-transferring cell aging reactions). Hence, for a more comprehensive assessment of EDLC performance, a parameter that deserves consideration is the specific energy. This parameter encompasses both capacitance and voltage, the latter being affected by overpotentials arising from cell resistance (increase of the IR drop, see reference^[9]). It is crucial to emphasize that in this context, the specific energy is calculated by integrating the instantaneous power (equation (3)). The multiplication of the instantaneous current and voltage allows for the inclusion of resistance-related effects. In this regard, Figure S3 of the Supporting Information compares the evolution of the specific energy as a function of cell voltage and temperature. However, to provide a clearer overview of the performance of the six investigated supercapacitors, we have illustrated their temperature-dependent progression of specific energy at a cell voltage of 3.0 V in Figure 4a. Three different trends can be distinguished: 1) A continuous decrease of available specific energy with increasing temperatures, which is the case for ACN, PN, and GVL. 2) An initial increase of specific energy, reaching its peak performance between 50 °C and 60 °C, followed by a decline, which can be observed for PC and BC. As mentioned before, this formation of a performance maximum is much more pronounced for BC. 3) A continuous increase of the energy output with increasing temperatures, which is shown by ADN. Furthermore, the specific power has been evaluated and is depicted in Figure S4 of the Supporting Information. Notably, the power shows less variation with the temperature than the specific energy. While resistance-related effects are not considered, the specific power is primarily influenced by the electrolyte's transport properties. Therefore, electrolytes that exhibit only moderate values of ionic conductivity and viscosity at room temperature experience a more significant change with the increase in temperature (ADN and BC) compared to those

that already demonstrate good performance at lower temperatures (ACN, PN, PC, and GVL). As previously shown for the specific energy, the temperature-dependent progression of specific power at a cell voltage of 3.0 V is shown in Figure 4b. Evidently, similar, although less pronounced, trends are observed. To provide a direct comparison of the specific energy with the specific power of a device under varying temperatures, Figure S5 of the Supporting Information shows a Ragone-like diagram. However, instead of varying the current density, the changing parameter is the temperature at a constant current rate of 1 A g⁻¹. The performance of specific energy and specific power at the upper voltage limits of 2.7 V, 3.0 V, and 3.4 V have been chosen as representatives.

As shown, the herein-presented testing protocol enables a fast screening process of the performance parameters of EDLCs containing different electrolytes. The incremental increase in temperature and voltage provides a large amount of data, which can be used to identify the optimal operation conditions of each respective device. This swift technique minimizes cell aging, permitting evaluation even under extremely challenging conditions. Furthermore, the obtained data sets further enable the examination of thermodynamic processes by entropometry. This technique, originally proposed by David C. Grahame in 1948, has found some application in the study of Li⁺ ion intercalation into host structures and double-layer formation on glassy carbon electrodes (GCE).^[10] However, corresponding thermodynamic investigations on EDLC full-cells using commercial activated carbon electrodes have not been reported so far. In this regard, it is important to highlight that the herein-reported values of enthalpy *H* and entropy *S* describe the relative change between the opposing electrodes (Figure 5). Various trends are consistent during the charging and discharging of EDLCs containing different electrolytes: On the one hand, throughout the charging process, entropy values increase and enthalpy values decrease. On the other hand, during the discharge process, entropy values decrease while enthalpy values increase. The change of entropy indicates an overall

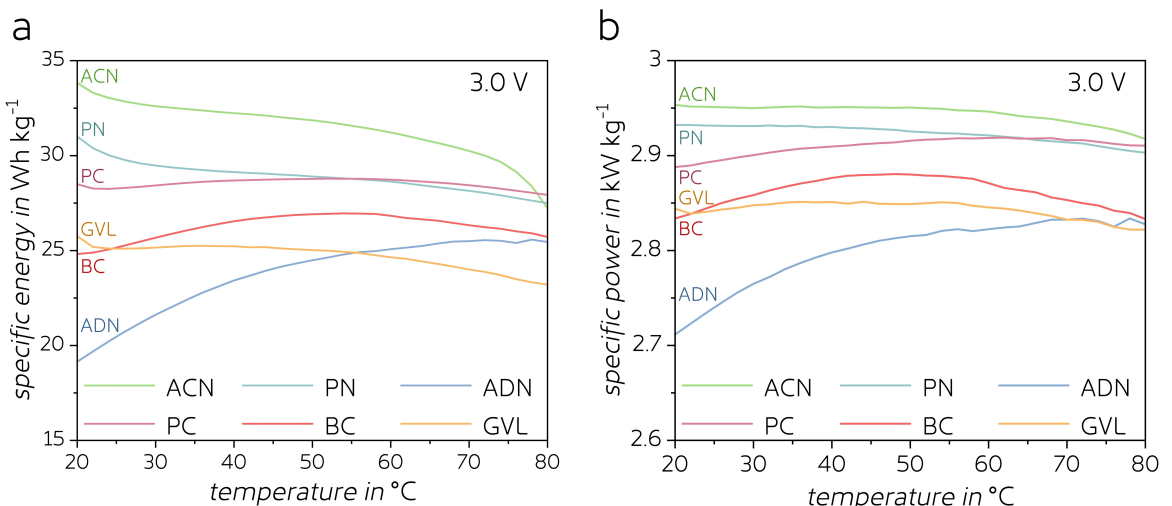


Figure 4. Evolution of the a) specific energy and b) specific power as a function of the applied temperature during galvanostatic cycling up to 3.0 V shown for the investigated electrolytes consisting of a 1 M solution of Pyr₁₁BF₄ in ACN (green), PN (turquoise), ADN (blue), PC (violet), BC (red) and GVL (orange).

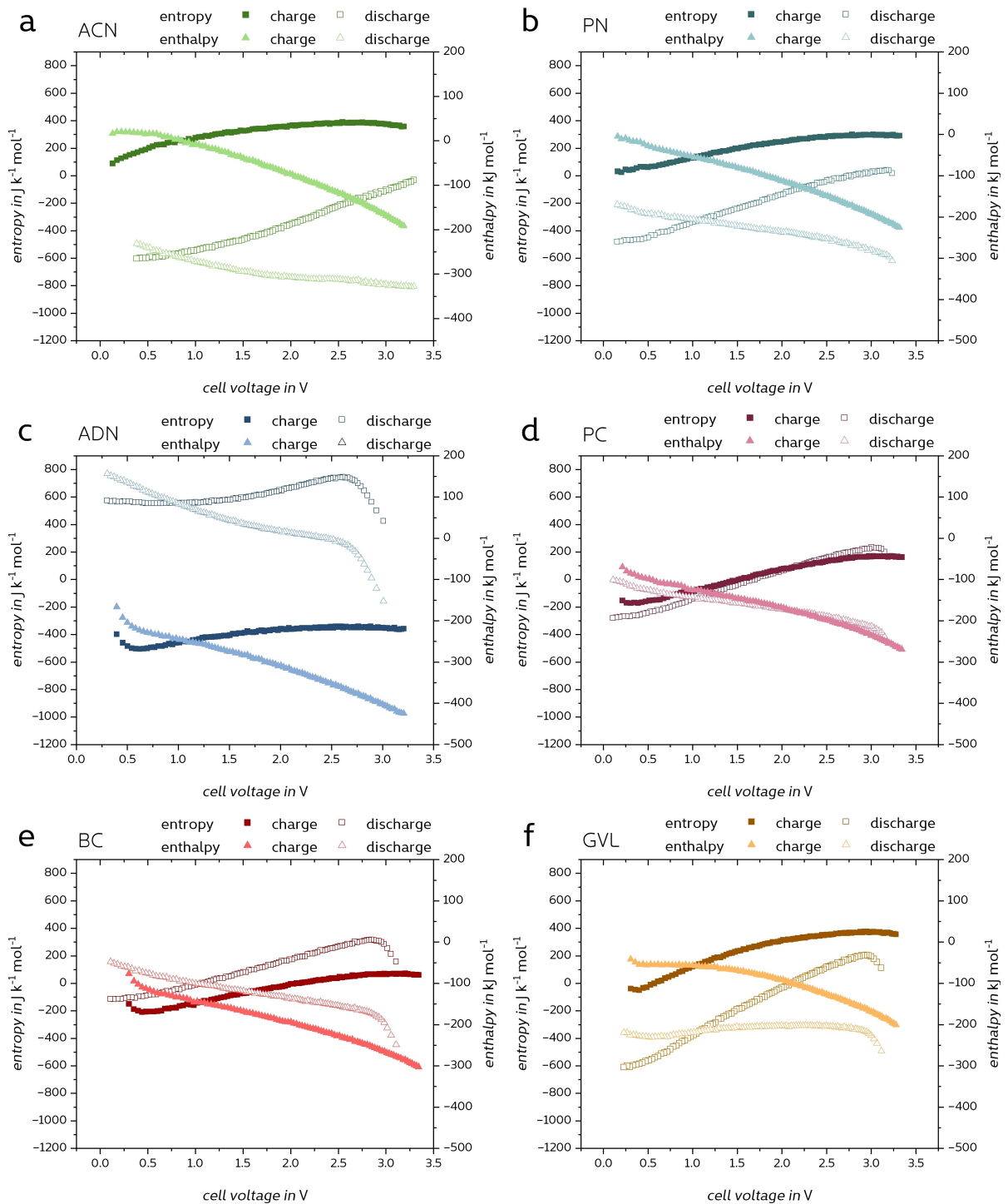


Figure 5. Thermodynamic analysis of symmetrical EDLC based on a one molar solution of 1 M $\text{Pyr}_{11}\text{BF}_4$ in a) ACN, b) PN, c) ADN, d) PC, e) BC, and f) GVL. Showing the evolution of enthalpy and entropy differences between the respective positive and negative AC electrodes as a function of the cell voltage. Calculated from galvanostatic cycling carried out at 1 A g^{-1} with increasing temperature in a range from 20°C to 80°C .

increase in states of disorder during the charging process and a decrease during discharging. Contrary to the expectation that polarization should cause a more pronounced ordering of ions at the electrode-electrolyte interphase and consequently decrease entropy (as observed for the double-layer formation on single GCEs^[10B]), such an effect has not been observed in this

context. This disparity may be caused by the different contributions of anion and cation accumulation at the opposing electrodes. The respective decrease in enthalpy during charging indicates either an increased heat consumption or a reduced heat release with progressing charge storage. The reverse is the case for the respective discharge process. Further, a clear

correlation between the absolute entropy and enthalpy values and the transport properties of the electrolytes is apparent. During the charge process, superior transport properties yield more positive values, while inferior transport properties correspond to more negative values. In this context, both enthalpy and entropy decrease in the following order: ACN > GVL > PN > PC > BC > ADN, similar to the trends observed for viscosity and ionic conductivity. This indicates an increase of charge ordering and an increase in heat consumption (or reduced heat release) with decreasing transport properties. Conversely, during the discharge phase, the scenario is reversed. Moreover, when comparing the different electrolytes, a significant disparity in entropy and enthalpy between the charge and discharge periods is evident. Generally, a significant difference is observed in the case of nitriles, whereas carbonate-based electrolytes exhibit very similar values during both charge and discharge periods. Specifically, for ACN and PN, the entropy and enthalpy values are higher during the charge than the discharge process, while the reverse is observed for ADN. Here, entropy and enthalpy are much higher during the discharge than during the charge period. Similarly, for PC, both entropy and enthalpy are higher during charge than during the discharge process, whereas the opposite is the case for BC. While discussing absolute values of enthalpy and entropy is challenging due to the inability to distinguish between individual processes occurring in EDLC full-cells, it is important to consider whether the magnitude of the measured entropy and enthalpy values are realistic. In the absence of similar thermodynamic investigations, a comparison with double-layer formation on single GCEs can be made. In this regard, Davey *et al.* observed the aforementioned ordering of ions at the electrode-electrolyte interphase during double-layer formation resulting in negative entropy values. Reaching reported entropy values of $-440 \text{ JK}^{-1} \text{ mol}^{-1}$ upon polarization and $1250 \text{ JK}^{-1} \text{ mol}^{-1}$ after sweep reversal. Corresponding enthalpy values of -165 kJ mol^{-1} and 300 kJ mol^{-1} were reached. These findings led to the proposal of ionic association between electrolyte ions and the surface of the GCE.^[10B] In the case presented here, values in a similar order of magnitude are reached, indicating plausibility.

3. Conclusions

In this work we showed that the herein presented T-dyn testing protocol allows the realization of a fast screening of the performance parameters of EDLCs with various electrolytes. The incremental increase in temperature and voltage allows the identification of optimal operational conditions for each device. It is important to highlight that the swift nature of this technique minimizes cell aging, facilitating evaluations even under highly demanding conditions. Thus, this technique enables easy comparison of the influence of various cell components, which shows great potential to be implemented as a routine screening process in research and development. Moreover, this protocol provides an additional avenue for the examination of thermodynamic processes through entropometry. It is crucial to emphasize that the reported values of

enthalpy and entropy characterize the relative change of states of a device containing two opposing electrodes. Thus, as EDLC full cells were used in this study, analyzing the individual contributions of the charge storage processes on entropy and enthalpy is not possible. Furthermore, *operando* T-Dyn measurements can also be adapted for other electrode materials, e.g. faradic or pseudocapacitive, as long as they provide sufficiently high power. However, even though the computation of the specific power and specific energy incorporate factors such as the internal resistance and non-linear dependency between the cell voltage and current, this testing protocol does not provide information regarding the long-term stability of a device at those conditions. Thus, in order to assess long-term behavior, supplementary aging tests need to be conducted.

Experimental section

Electrolyte preparation

The solvents acetonitrile (ACN, CAS 75-05-08, purity $\geq 99.8\%$, Sigma-Aldrich), adiponitrile (ADN, CAS 111-69-3, purity $\geq 99\%$, Sigma-Aldrich), propionitrile (PN, CAS 107-12-0, purity $\geq 99\%$, Sigma-Aldrich), propylene carbonate (PC, CAS 108-32-7, purity $\geq 99.7\%$, Sigma-Aldrich), butylene carbonate (BC, CAS 4437-85-8, purity $\geq 98\%$, TCI Chemcials) and γ -valerolactone (GVL, CAS 108-29-2, purity $\geq 99\%$, Sigma-Aldrich) were dried using a molecular sieve (3 Å or 4 Å) to reduce the respective water content below 20 ppm, which has been confirmed by Karl-Fischer-Titration. The salt dimethylpyrrolidinium tetrafluoroborate (Pyr₁BF₄, CAS 69444-51-5, purity $\geq 99\%$, IoLiTec) has been dried in a vacuum glass oven at 80 °C and 10⁻² mbar for 24 h before use. As electrolytes a one molar solution of the salt and the respective solvent has been produced and stored inside an argon filled glovebox. The respective chemical structures of the electrolyte components are shown in Scheme 1.

Physicochemical properties of the electrolytes

The ionic conductivities of the respective electrolytes have been determined within the temperature range of -10 °C to 80 °C using a Binder KB 53 climatic chamber and a BioLogic MPG-2 potentiostat according to a procedure described before.^[11] Viscosity measurements have been performed by an Anton-Paar MCR 102 rotational viscometer with a sheer rate of 1000 s⁻¹. Here, 500 µL were used for the measurement within the same temperature range as before, following a procedure described in an earlier publication.^[11] Thermogravimetric analysis (TGA) has been performed utilizing a PerkinElmer TGA 4000 with an applied temperature ramp of 10 °min⁻¹ (30–550 °C) according to a procedure described elsewhere.^[6F]

Cell assembly

The electrochemical measurements performed in this study were conducted using activated carbon electrodes provided by Skeleton Technologies. To ensure that the experimental setup was consistent, one side of the double-sided activated carbon coating was removed using ethanol before application. This resulted in electrodes with a mass loading of 8.24 mg cm⁻² and an electrode area of 1.13 cm². The measurements were performed in Swagelok-type cells with a two-electrode configuration using two identical electrodes separated by a 520 µm Whatman GF/D glass fiber disk soaked

with 120 μL of the respective electrolyte. The cells were assembled in a MBRAUN LABmaster pro glove box, which was filled with argon to maintain a H_2O and O_2 content of less than 1 ppm. To limit human error and enhance cell performance, after assembly, all cells have been pressed at 20 N cm^{-2} and were subjected to galvanostatic precycling at 1 A g^{-1} between 0 V and 2.0 V for 500 cycles.

Operando temperature dynamic measurements

Operando temperature dynamic measurements (T-dyn) were performed according to the experimental procedure previously reported by L. Köps et al. (illustrated in Scheme 2).^[6G] In summary, two types of electrochemical techniques were performed inside a controlled temperature dynamic environment: electrochemical impedance spectroscopy (EIS) and galvanostatic charge-discharge (GCD).

Utilizing a Binder KB 53 climatic chamber and a BioLogic MPG-2 potentiostat operando temperature dynamic electrochemical impedance spectroscopy (T-dyn EIS) has been performed at open circuit voltage within a temperature range of 20–80 °C. Impedance spectra were obtained at every 1 °C interval within a frequency range of 100 kHz – 10 mHz.

Operando temperature dynamic galvanostatic charge-discharge (T-dyn GCD) was conducted in the same experimental setup. The cells were cycled five times within a voltage range of 0–2.7 V, before increasing the upper voltage limit by 50 mV after each five-cycle set until reaching 3.4 V. This process was repeated every 2 °C, beginning from 20 °C. The cells were conditioned in the same procedure as described before.

Data evaluation

The specific capacitance C [F g^{-1}] during T-dyn impedance spectroscopy was determined using the formula:

$$C = \frac{-1}{2 \pi f |Z| m} = \frac{-1}{2 \pi f \sqrt{\text{Im}(Z)^2 + \text{Re}(Z)^2} m} \quad (1)$$

where f represents the frequency, $|Z| [\Omega]$ is the modulus function of the total impedance, $\text{Im}(Z)$ and $\text{Re}(Z)$ respectively represent the imaginary and real part of the impedance, and $m [\text{g}]$ is the active mass of the electrode material. The time $t [\text{s}]$ corresponds to the reciprocal value of the applied frequency f , so $t = f^{-1}$. Thus, t indicates the needed charge-discharge time of the corresponding capacitor. The specific capacitance presented in the study corresponds to the capacitance of the cell containing two symmetrical electrodes.

According to a procedure described elsewhere, the maximum power P_{\max} [W] and maximum energy E_{\max} [Wh] have been determined for the discharge period during T-dyn GCD measurements.^[9] The instantaneous power $p(t)$ [W] was obtained from the product of the instantaneous voltage $v(t)$ [V] and current $i(t)$ [A], which represent the voltages and currents at any given moment in time. Subsequently, P_{\max} corresponds to the maximum of the modulus function of $p(t)$ of the discharge period.

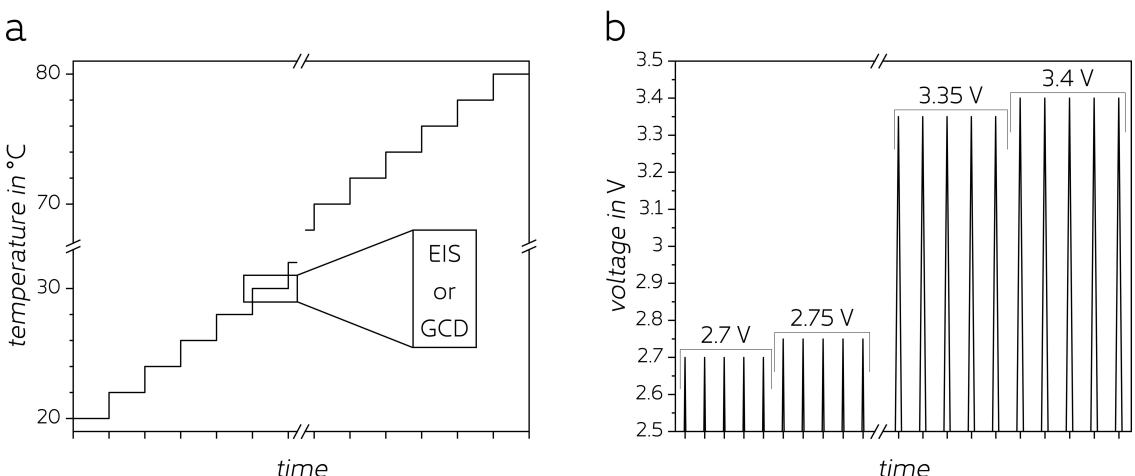
$$P_{\max} = \max\{|p(t)|\} = \max\{|v(t)i(t)|\} \quad (2)$$

Similarly, E_{\max} has been evaluated by integration of $p(t)$ during the discharge period:

$$E_{\max} = \int_{t_0}^{t_n} p(t) dt = \int_{t_0}^{t_n} v(t)i(t) dt \quad (3)$$

where t_0 is the initial time [s] and t_n [s] is the final time of the discharge.

Thermodynamic differences of the double-layer formation processes in different electrolyte systems have been calculated by entropymetry.^[10] To compare different electrolyte systems, it is important to guarantee that the same amount of charge q accumulates on the electrode surfaces for each temperature T . Thus, in a first step the cell voltage V [V] as a function of the temperature has been determined for each value of cumulative charge. Subsequently, the enthalpy H (J mol^{-1}) and the entropy S ($\text{JK}^{-1}\text{mol}^{-1}$) are determined by linear extrapolation of the cell voltage versus the temperature.



Scheme 2. Schematic illustrations of experimental procedures: a) Temperature profile during temperature dynamic electrochemical impedance spectroscopy (EIS) and galvanostatic charge-discharge measurements with incremental temperature steps of 2 °C. This controlled temperature staircase allows for a comprehensive analysis of the electrochemical processes at different thermal conditions. b) Voltage profiles of the performed charge-discharge measurements at 1 A g^{-1} . The voltage limit for the charge and discharge cycles is sequentially increased each five cycles by 50 mV starting from 2.7 V until reaching 3.4 V. Reprinted according to the terms of the Creative Commons CC-BY license.^[6G]

$$dV(T)_{q=const.} = -\frac{dH}{nF} + T \frac{dS}{nF} \quad (4)$$

With n representing the stoichiometry of the charge transfer process (which has been set to 1), and the Faraday's constant F ($96486.7 \text{ J K}^{-1} \text{ mol}^{-1}$), the variation of enthalpy dH can be determined by the vertical intercept of the potential change as a function of the temperature $dE(T)$ and the variation of enthalpy dS by its slope. A more detailed description of this technique is provided by Davey *et al.*^[108]

Acknowledgements

The financial support from the Friedrich-Schiller-University Jena (FSU Jena), the Deutsche Forschungsgemeinschaft (DFG) within the project "New Electrolytes for Capacitive Electrochemical Storage" (BA4956/16-1) and the Bundesministerium für Wirtschaft und Klimaschutz (BMWK) within the project "SUPREME" (03EI6060B) is gratefully acknowledged. Further S.W.D. acknowledges the Australia-Germany Joint Research Cooperation Scheme (ID: 57654993) for travel funding. Open Access funding enabled and organized by Projekt DEAL.

Conflict of Interests

The authors declare no conflict of interest.

Data Availability Statement

The data that support the findings of this study are available from the corresponding author upon reasonable request.

Keywords: supercapacitor • electrolyte • energy • entropymetry • power,

- [1] A. A. Brandt, A. Balducci, *J. Power Sources* **2014**, *250*, 343–351; B. C. Schütter, S. Pohlmann, A. Balducci, *Adv. Energy Mater.* **2019**, *9*, 1900334;

C. F. A. Kreth, A. Balducci, in *Reference Collection in Chemistry, Molecular Sciences and Chemical Engineering*, Elsevier Inc., **2023**.

- [2] A. R. Carter, A. Cruden, P. J. Hall, *IEEE Trans. Veh. Technol.* **2012**, *61*, 1526–1533; B. L. Kouchachvili, W. Yaici, E. Entchev, *J. Power Sources* **2018**, *374*, 237–248; C. R. T. Meyer, R. A. DeCarlo, S. Pekarek, *Asian Journal of Control* **2016**, *18*, 150–165; D. Z. Song, J. Li, J. Hou, H. Hofmann, M. Ouyang, J. Du, *Energy* **2018**, *154*, 433–441; E. T. P. Sumangala, M. S. Sreekanth, A. Rahaman, in *Handbook of Nanocomposite Supercapacitor Materials III: Selection* (Ed.: K. K. Kar), Springer International Publishing, Cham, **2021**, pp. 367–393; F. K. V. G. Raghavendra, R. Vinoth, K. Zeb, C. V. V. Muralee Gopi, S. Sambasivam, M. R. Kumara, I. M. Obaidat, H. J. Kim, *J. Energy Storage* **2020**, *31*, 101652; G. D. Lasrado, S. Ahankari, K. K. Kar, in *Handbook of Nanocomposite Supercapacitor Materials III: Selection* (Ed.: K. K. Kar), Springer International Publishing, Cham, **2021**, pp. 329–365.
- [3] L. Köps, F. A. Kreth, D. Leistenschneider, K. Schutjajew, R. Gläßner, M. Oschatz, A. Balducci, *Adv. Energy Mater.* **2023**, *13*, 2203821.
- [4] L. Köps, P. Ruschhaupt, C. Guhrenz, P. Schlee, S. Pohlmann, A. Varzi, S. Passerini, A. Balducci, *J. Power Sources* **2023**, *571*, 233016.
- [5] A. Z. Lin, E. Goikolea, A. Balducci, K. Naoi, P. L. Taberna, M. Salanne, G. Yushin, P. Simon, *Mater. Today* **2018**, *21*, 419–436; B. K. S. Teoh, M. Melchiorre, F. A. Kreth, A. Bothe, L. Köps, F. Ruffo, A. Balducci, *ChemSusChem* **2023**, *16*, e202201845.
- [6] A. L. Köps, F. A. Kreth, A. Bothe, A. Balducci, *Energy Storage Mater.* **2022**, *44*, 66–72; B. H. V. T. Nguyen, A. B. Faheem, K. Kwak, K.-K. Lee, *J. Power Sources* **2020**, *463*, 228134; C. A. Bothe, S. E. M. Pourhosseini, P. Ratajczak, F. Beguin, A. Balducci, *J. Power Sources* **2021**, *496*, 229841; D. L. H. Hess, A. Balducci, *Electrochim. Acta* **2018**, *281*, 437–444; E. S. Pohlmann, A. Balducci, *Electrochim. Acta* **2013**, *110*, 221–227; F. A. Bothe, A. Balducci, *Electrochim. Acta* **2021**, *374*, 137919; G. L. Köps, F. A. Kreth, M. Klein, A. Balducci, *J. Power Sources* **2023**, *581*, 233480.
- [7] A. E. Pameté, L. Köps, F. A. Kreth, S. Pohlmann, A. Varzi, T. Brousse, A. Balducci, V. Presser, *Adv. Energy Mater.* **2023**, *23*, 2301008; B. F. A. Kreth, L. H. Hess, A. Balducci, *Energy Storage Mater.* **2023**, *56*, 192–204.
- [8] H. Wang, L. Pilon, *Electrochim. Acta* **2012**, *63*, 55–63; X. Ren, P. G. Pickup, *J. Electroanal. Chem.* **1994**, *372*, 289–291; F. Lufrano, P. Staiti, M. Minutoli, *J. Power Sources* **2003**, *124*, 314–320; L. E. Helseth, *J. Energy Storage* **2021**, *35*, 102304.
- [9] L. Köps, P. Zaccagnini, C. F. Pirri, A. Balducci, *Journal of Power Sources Advances* **2022**, *16*, 100098.
- [10] A. J. R. Dahn, R. R. Haering, *Can. J. Phys.* **1983**, *61*, 1093–1098; B. S. B. Davey, A. P. Cameron, K. G. Latham, S. W. Donne, *Journal of Power Sources Advances* **2021**, *10*, 100062; C. R. Yazami, Y. Reynier, B. Fultz, *ECS Trans.* **2006**, *1*, 87; D. D. C. Grahame, *J. Chem. Phys.* **1948**, *16*, 1117–1123.
- [11] L. H. Heß, A. Balducci, *ChemSusChem* **2018**, *11*, 1919–1926.

Manuscript received: December 8, 2023

Revised manuscript received: January 19, 2024

Accepted manuscript online: January 22, 2024

Version of record online: February 6, 2024